Characterizing Trabecular Bone Properties near the Glenohumeral Joint Following Brachial Plexus Birth Injury

Emily B. Fawcett[a,1], Carolyn M. McCormick[a,1], Austin F. Murray[a], Dustin L. Crouch[b], PhD, Katherine R. Saul[b], PhD, and Jacqueline H. Cole [a,*], PhD

[1] These authors contributed equally to this work.

[a] Joint Department of Biomedical Engineering, University of North Carolina, Chapel Hill, NC, and North Carolina State University, Raleigh, NC, USA

[b] Mechanical and Aerospace Engineering, North Carolina State University, Raleigh, NC, USA

*Corresponding Author:
Jacqueline H. Cole
Joint Department of Biomedical Engineering
University of North Carolina and North Carolina State University
911 Oval Drive
Campus Box 7115
Raleigh, NC 27695-7115
Tel: 919-515-5955
Fax: 919-513-3814
jacquecole@ncsu.edu

1   **Abstract**

2   Brachial plexus birth injury (BPBI) causes functional arm impairment in 30-40% of those affected

3   due to altered loading on the glenohumeral joint. While gross morphological osseous deformities

4   have been seen in the humerus and scapula, alterations in the underlying trabecular bone

5   microstructure and mineralization are not clear. Using a murine model of BPBI, trabecular bone

6   alterations were explored in the proximal humerus and distal scapula, which surround the

7   articulating surface of the joint. Samples were scanned using micro-CT, reoriented, and analyzed

8   for standard trabecular metrics. The regions of interest closest to the articulating surface showed

9   the greatest detriments. In the scapula, the scapular neck region showed less robust trabecular bone

10   in the neurectomy group with decreased BV/TV (p=0.001), BMD (p=0.001), Conn.D (p=0.006),

11   Tb.N (p<0.0001), and DA (p=0.033), and increased Tb.Sp (p<0.0001) compared to sham. In the

12   humerus, the epiphysis showed less robust trabecular bone in neurectomy group, but to a much

13   lesser extent than the scapular neck. The neurectomy group showed reduced BMD (p=0.007) and

14   Tb.N (p=0.029) compared to sham. Data suggest deformities are worse near the articulating

15   surface, likely due to the greater amount of mechanical loading. The reduction in trabecular

16   microstructure and mineralization may compromise bone strength of the affected limb following

17   BPBI. Further investigation of the underlying trabecular bone deformities following injury are

18   necessary to eventually inform better treatments to limit the development of deformities.

19

20   **Keywords**

21   brachial plexus birth injury, trabecular microstructure, bone mineral density, glenohumeral joint

Introduction

Functional impairment of the arm is permanent in 30-40% of children who sustain brachial plexus birth injuries (BPBI) during difficult childbirth (Pondaag, 2004).[1] Secondary glenohumeral dysplasia in the affected limb can result from injury (Waters 1998) and may alter the mechanical loading of the joint, which is critical for normal bone and joint development. Regions in the glenohumeral joint experience abnormal growth and macrostructural deformities after BPBI[2–6] (Al-Qattan 2003, Nikolaou 2011, Crouch 2014, Crouch 2015, Cheng 2015), and are comprised primarily of cancellous bone, which plays an integral role in transferring joint loading along the bone and is known to adapt to altered loads (Wolff, 1892/1986; Frost, 1994).

Trabecular bone loss has been observed in many reduced loading scenarios, such as spaceflight[7] (Vico *et al.*, 2000), prolonged bedrest[8] (Kazakia *et al.*, 2014), and spinal cord injury (Eser *et al.*, 2004).[9] However, the nature and extent of trabecular bone changes after BPBI are not well understood. While no human BPBI study has examined bone microstructural properties, several studies using murine BPBI models have reported trabecular bone detriments in the humeral head, with fewer and thinner trabeculae and greater separation compared to contralateral limb and sham control groups[10–12] (Kim, 2009; Kim, 2010; Potter, , 2014). These trabecular changes were observed in conjunction with global musculoskeletal changes, including humeral anteversion and glenoid retroversion[10,11] (Kim *et al.*, 2009; Kim *et al.*, 2010), as well as decreased supraspinatus muscle volume[10–12] (Kim *et al.* 2009; Kim *et al.*, 2010; Potter *et al.*, 2014). Beyond morphological changes, the elastic modulus and overall strength of the humeral head decreased (Potter 2014).[12] However, previous animal studies have not characterized trabecular changes throughout the entire glenohumeral region, particularly in the scapula glenoid region and humeral metaphysis, nor have they examined the relationship between changes in glenohumeral macrostructure and changes in

45 the underlying trabecular microstructure. In addition, tissue mineral density is related to elastic

46 modulus, which has been seen to decrease. Yet tissue mineral density has not been characterized

47 following BPBI. This information could reveal regions of the glenohumeral joint that may be

48 especially susceptible to BPBI-induced changes in trabecular bone, ultimately informing better

49 treatment strategies to mitigate the macrostructural deformities and address the deficits in arm

50 function experienced by human patients.

51 Mechanical loading is well established as a critical determinant of bone morphology

52 throughout development (Frost, 1994; Turner, 1998).[13,14] Altered mechanical loading has been

53 proposed as a major contributing factor in the development of osseous deformities in the

54 glenohumeral joint affected by BPBI. Osseous deformities reported in clinical studies include

55 flattening of the humeral and posterior subluxation relative to the scapula (Reading 2012, Waters

56 1998).[15,16] Most scapular deformities have been identified in the glenoid fossa, including glenoid

57 retroversion, declination, loss of glenoid concavity, and pseudoglenoid formation (Waters

58 1998).[16] Computational musculoskeletal models developed from animal studies have determined

59 that, when compared to a normal developing shoulder, the BPBI glenohumeral joint experiences

60 increased posteriorly directed, compressive loads, due to impaired growth of surrounding muscles

61 (Crouch, 2014, Cheng, 2015).[4,6] Indications of altered mechanical loading following BPBI

62 motivate further investigation of the glenohumeral trabecular microstructure and mineralization,

63 which bears primary responsibility for distributing loads in the shoulder joint.

64 The purpose of this study was to characterize microstructural features in the underlying

65 trabecular bone near the articulating glenohumeral joint (e.g., humeral epiphysis and metaphysis,

66 scapular regions near the glenoid) using an established rat model of BPBI (Li *et al.*, 2008; Nikolaou

67 *et al.*, 2015).[17,18] Given the supporting evidence from other scenarios of altered loading and the

4

68   remarkable skeletal dysplasia known to occur in clinical cases of BPBI, we hypothesized that

69   trabecular tissue mineral density and microstructure in the affected shoulder are compromised

70   during postnatal development following BPBI.

71

72   **Methods**

73   Study Design

74   This study was performed using humeri and scapulae obtained from a previous study

75   (Crouch 2015).[19] All animal procedures were approved by the Institutional Animal Care and Use

76   Committee at the Wake Forest School of Medicine. Sixteen Sprague Dawley rat pups (Harlan

77   Laboratories, Indianapolis, Indiana) were grouped according to surgical intervention implemented

78   five days after birth: neurectomy and sham (n=8 each) (Figure 1).

79   In the neurectomy group, a postganglionic injury was surgically induced in the left forelimb

80   using an established model (Li 2008),[17] and the right forelimb was kept completely intact as a

81   control. The rats were anesthetized with inhaled isoflurane, and a small transverse infraclavicular

82   incision was made, splitting the left pectoralis major muscle to expose the brachial plexus. The left

83   C5 and C6 nerve roots and the upper trunk of the brachial plexus were transected distal to the

84   dorsal root ganglion. The wound was irrigated with saline and closed with 6-0 nylon suture. The

85   sham group received a similar surgery with incision through the left pectoralis major muscle, but

86   the brachial plexus was not transected, and the right forelimb was kept completely intact.

87   After eight weeks, the rats were sacrificed, and the left (affected) and right (unaffected)

88   scapulae and humeri were harvested. The bones were fixed in 10% neutral buffered formalin for

89   48 hours and then immersed in 70% ethanol for storage. Two scapulae per group and one humerus

90   per group were damaged during the original dissection, leaving n = 6 left and right scapulae and n

91   = 7 left and right humeri for this study.

92

93   <u>Micro-Computed Tomography</u>

94   Trabecular bone density and microstructure were assessed with quantitative micro-

95   computed tomography (micro-CT). The bones were scanned in 70% ethanol using a 0.5-mm Al

96   filter, 45 kVp and 177 μA, 800-ms integration time, 1,000 projections per rotation, and no frame

97   averaging (μCT 80, SCANCO Medical AG, Brüttisellen, Switzerland). Density measurements

98   were calibrated using the SCANCO hydroxyapatite calibration phantom, and a threshold of 441

99   mg/cm^3 (3891 Hounsfield units) was applied for bone. The scans were reconstructed at an isotropic

100   voxel size of 10 μm and reoriented for consistent anatomical alignment. Trabecular bone volumes

101   of interest (VOIs) were selected near the glenohumeral joint, which was expected to be most

102   affected following nerve injury. Three VOIs in the glenoid fossa region of the scapula and two

103   VOIs in the proximal humerus were selected by manually contouring the trabecular bone in a series

104   of slices and then using automated morphing interpolation across these contours to create the

105   volumes (Figure 2). All VOI lengths were chosen based on the maximum possible length in each

106   region for the smallest bone.

107   The three scapular VOIs were defined in secondary ossification centers formed during

108   postnatal development (Kothary *et al.*, 2014).[20] The first scapular VOI (*zone 1*) was 6.5% of the

109   total scapular length, defined as the distance from the beginning of the glenoid region to the farthest

110   point of the proximal end. This VOI was positioned in the subcoracoid secondary ossification

111   center, beginning next to the articular surface and extending proximally along the scapular spine

112   axis toward the superior glenoid physis. The second scapular VOI (*zone 2*) was 1.5% of the total

113   scapular length and defined in the upper glenoid secondary ossification center, beginning inferior

114   to the superior glenoid physis and next to the articular surface extending proximally along the

115   scapular spine. The third VOI (*zone 3*) was 7.5% of the total scapular length and was defined

116   within the scapular neck, beginning next to the physis running across the width of the neck and

117   extending proximally. The first humeral VOI was 12.5% of the total humeral length and defined

118   in the epiphysis, beginning inferior to the articular surface and extending distally toward the

119   proximal growth plate. The second humeral VOI was 5% of the total humeral length and defined

120   in the metaphysis, beginning inferior to the proximal growth plate and extending distally toward

121   the diaphysis. For each VOI, standard trabecular bone metrics were calculated using the SCANCO

122   analysis software, including bone volume fraction (BV/TV), bone mineral density (BMD), tissue

123   mineral density (TMD), connectivity density (Conn.D), trabecular number (Tb.N), mean

124   trabecular thickness (Tb.Th) and separation (Tb.Sp) using direct 3D methods (Hildebrand and

125   Rüegsegger 1997),[21] and degree of anisotropy (DA) (Bouxsein *et al*., 2010).[22]

126

127   <u>Statistical Analyses</u>

128   Four sets of analyses were performed. For analysis 1, limb comparisons for trabecular bone

129   metrics were examined between affected and unaffected limbs within each group (sham,

130   neurectomy) using paired t-tests with Welch's correction for unequal variances. For analysis 2,

131   group comparisons for the affected-to-unaffected ratios were examined between the neurectomy

132   and sham groups using unpaired t-tests with Welch's correction for unequal variances. For analysis

133   3, anatomical site relationships were examined between the scapula and humerus metrics using

134   linear correlations. These relationships were evaluated using both the microstructural metrics from

135   this study and the macrostructural metrics from the previous study using these same bones

136   (humeral head width, thickness, and curvature; glenoid inclination and curvature) (Crouch

137   2015).[5] For analysis 4, length-scale relationships between the glenohumeral joint macrostructure

138   and underlying trabecular microstructure were assessed by stepwise multiple regression with

139   forward selection, using Schwarz Bayesian information criterion to determine which trabecular

140   microstructural properties (predictor variables) best explained the variability in the macrostructural

141   measurements in the humeral head (width, thickness, and curvature) and glenoid fossa (inclination

142   and curvature). Microstructural values from the humeral epiphysis and glenoid zone 3 (Z3) were

143   used for the correlations and multiple regressions, since these regions were closest to, and thus

144   most relevant to, the articulating glenohumeral joint. Analyses 1, 2, and 3 were completed with

145   Prism 6 (GraphPad Software, Inc., La Jolla, CA), and analysis 4 was completed with SAS 9.4 (SAS

146   Institute Inc., Cary, NC). Significance was defined as $p < 0.05$, and trends were defined as $p <$

147   0.08.

148

149   **Results**

150   Limb Comparisons

151   *Scapula*

152   For the neurectomy group, trabecular bone density and microstructure were altered in the

153   scapula of the affected limb when compared to the contralateral unaffected limb (Table 1, Figure

154   3). Bone volume fraction was decreased 21-26% in zones 2 and 3 and tended to decreased about

155   18% in zone 1, and bone mineral density was decreased 19-24% in zones 1, 2, and 3, indicating a

156   reduction in bone mass on the affected side. Zone 2 also tended to show decreased tissue mineral

157   density, indicative of material change. In zones 1 and 3, trabecular number was reduced by

158   approximately 20% and trabecular separation was increased 35-44% on the affected side. Zone 2

8

159 had decreased trabecular thickness by approximately 18%. The alterations in trabecular

160 architecture indicate less robust trabecular bone in zones 1 and 3 on the affected side compared to

161 zone 2. In addition, zone 1 portrayed a decrease in anisotropy of about 10%.

162   The sham group also experienced some differences in trabecular bone microstructure for

163 zones 2 and 3 of the scapula on the affected side when compared to the contralateral limb (Table

164 1, Figure 3). Specifically, zone 2 had reduced bone volume fraction and bone mineral density by

165 about 5%, indicating decreased bone mass. In addition, zone 3 had a 12% increase in connectivity

166 density and tended to have a 5% increase in trabecular number and 5% decrease in trabecular

167 separation. However, the bone on the affected sides in the sham group were much less affected

168 than those in the neurectomy group.

169

170 *Humerus*

171   The neurectomy group exhibited less robust trabecular bone in the affected epiphysis when

172 compared to the unaffected epiphysis (Table 2, Figure 4a). Bone volume fraction and bone mineral

173 density were reduced by approximately 19% and 24% respectively, revealing loss of bone mass in

174 the affected limb. Related to material changes, tissue mineral density tended to decrease by 4% on

175 the affected side. In addition, trabecular separation was increased by about 90% on the affected

176 side and trabecular number tended to decrease by 33%, indicating less robust trabecular

177 architecture. In the metaphysis, less alterations were present in the affected limb (Table 2, Figure

178 4b). Trabecular material was significantly altered with a 6% reduction in tissue mineral density,

179 and connectivity density was increased by approximately 112%.

180   Unlike in the neurectomy group, in the sham group, there were no significant deformities

181   found in the epiphysis of the affected side when compared to the contralateral limb. However, the

182   metaphysis region of the affected side portrayed increased connectivity density by 139%,

183   trabecular number by 16%, and degree of anisotropy by 45%, and decreased trabecular separation

184   by 18%. Trabecular thickness also tended to decrease by 6%, all indicating different trabecular

185   architecture between limbs.

186

187   <u>Group Comparisons</u>

188   *Scapula*

189   In zone 1 and 2 of the glenoid fossa region, few trabecular metrics differed significantly

190   between the neurectomy and sham groups (Figure 4a-b). Zone 1 showed lower bone volume

191   fraction (-19.6%, p=0.039), bone mineral density (-19.8%, p=0.018), and trabecular number (-

192   20.6%, p=0.028), and increased trabecular separation (+38.8%, p=0.020) when compared to sham.

193   Zone 2 showed lower bone volume fraction (-21.3%, p=0.001), bone mineral density (-20.0%,

194   p=0.002), and tissue mineral density (-3.1%, p=0.047) compared to sham. Glenoid trabecular bone

195   was most altered in zone 3 following neurectomy (Figure 4c). Bone volume fraction and bone

196   mineral density were reduced (-21.2%, p=0.001; -22.8%, p=0.001 respectively) compared to sham,

197   representing decreased bone mass following injury. Trabecular architecture was also less robust,

198   indicated by a decrease in connectivity density (-28.7%, p=0.006), trabecular number (-24.5%,

199   p<0.0001), and degree of anisotropy (-11.76%, p=0.033), and an increase in trabecular separation

200   (+45.2%, p<0.0001).

201

10

202   *Humerus*

203   The epiphyseal region shows few altered trabecular metrics in the neurectomy group

204   (Figure 5a). Specifically, there was a decrease in bone volume fraction (+7.76%, p=0.024), bone

205   mineral density (-16.3%, p=0.007), and trabecular number (-0.3%, p=0.029), and a trend towards

206   decreased connectivity density (-34.0%, p=0.051). and increased trabecular separation (+39.4%,

207   p=0.057) when compared to sham. These altered metrics indicate reduction in bone mass and less

208   robust trabecular architecture.

209   In the metaphyseal region, there were no significant differences between the neurectomy

210   and sham group (Figure 5b). There were also no trends towards less robust trabecular bone in the

211   neurectomy group compared to sham, suggesting no alterations due to injury.

212

213   Anatomical Site Relationships

214   Correlations were present between microstructural regions near articulating glenohumeral

215   surfaces (Table 3). Some correlations were present between microstructural regions near the

216   articulating glenohumeral surfaces (Table 3). Tissue mineral density in scapular zone 3,

217   representative of material properties, correlated with epiphyseal trabecular bone architecture

218   metrics and tended to correlate with epiphyseal bone mas metrics. Specifically, scapular zone 3

219   tissue mineral density positively correlated with epiphyseal connectivity density (r=0.913,

220   p=0.030) and trabecular number (r=0.946, p=0.015), and negatively correlated with trabecular

221   separation (r= -0.978, p=0.004). Tissue mineral density also tended to positively correlate with

222   bone volume fraction (r=0.837, p=0.077) and bone mineral density (r=0.816, p=0.092).

11

223   In the epiphysis, degree of anisotropy correlated with some trabecular bone architecture

224   metrics and tended to correlate with bone mass metrics, all from scapular zone 3. Specifically,

225   degree of anisotropy positively correlated with zone 3 trabecular number (r=0.973, p=0.005) and

226   negatively correlated with zone 3 trabecular separation (r= -0.960, p=0.010). The degree of

227   anisotropy in the epiphysis also tended to positively correlate with zone 3 bone volume fraction

228   (r=0.873, p=0.054) and bone mineral density (r=0.84, p=0.075).

229

230   <u>Length-Scale Relationships</u>

231   Nearly all macrostructural bone measurements (glenoid curvature and inclination, humeral

232   head width, thickness, and curvature) were linearly correlated with at least one microstructural

233   bone metric (Table ##). Multiple regression models included measurements from both groups

234   (sham and neurectomy). Changes in glenoid curvature were best explained by BV/TV and TMD,

235   respectively. Glenoid inclination variability was best explained by Tb.Sp, Conn.D, Tb.N, and SMI.

236   Changes in humeral head thickness were best explained by DA, Tb.Th, TMD, and Tb.Sp. Variation

237   in humeral head curvature was best explained by Conn.D. Humeral head width did not appear to

238   be significantly affected by any particular microstructural parameter.

239

240   **Discussion**

241   The goal of this study was to investigate whether trabecular bone density and

242   microstructure are altered in regions near the glenohumeral joint following brachial plexus birth

243   injury in rats. Our findings show clear differences in the trabecular bone density and microstructure

244   for limbs affected by neurectomy compared to both their unaffected contralateral control limb and

245   sham control. The most profound differences in trabecular metrics occurred in the articulating

246 regions of the glenohumeral joint – the humeral epiphysis and the glenoid zone 3. The scapula was

247 affected in more parameters of trabecular bone density and microstructure relative to the humerus.

248 Our findings in the underlying trabecular bone near the glenohumeral joint provide broader context

249 for the global musculoskeletal deformities known to occur in children with BPBI.

250 Prior work in murine models of BPBI have reported microstructural changes to the humeral

251 epiphysis that worsen over time, but the parameters affected differ from the current report. For

252 example, a cross-sectional study in a CD-1 mouse model of BPBI employing the same type of

253 neurectomy at 24 hours following birth reported a 22.2% reduction in Tb.Th in the humeral

254 epiphysis of the affected limb relative to the contralateral limb and 17.7% relative to sham at four

255 weeks post-injury. After twelve weeks, Tb.Th reduced further to 42.2% relative to the contralateral

256 limb and 50% relative to sham (Kim *et al.*, 2010). [13] In contrast, we observed reduced epiphyseal

257 BV/TV and BMD, increased Tb.Sp, and a trend towards decreased TMD and Tb.N in the affected

258 neurectomy limb compared to the contralateral control limb and reduced BMD, Conn.D, and Tb.N

259 compared to sham, but no significant changes to Tb.Th. These trabecular bone losses indicate that

260 BPBI compromises bone microstructure shortly after injury and more severely over time,

261 suggesting that timing of post-injury treatment is critical to bone health. These results, combined

262 with the examination of the metaphyseal region and regions of the scapula help reveal the location

263 of the greatest disparities in affected shoulders compared to contralateral or sham shoulders.

264 Our group is the first to investigate the trabecular microstructure following BPBI in the

265 humeral metaphysis and regions of the scapula within the glenoid fossa. This study found that

266 there was a significant reduction in TMD of the affected neurectomy limb compared to the

267 contralateral limb in both the epiphysis and metaphysis, and a significant reduction in TMD of the

268 neurectomy group in the epiphysiscompared to sham. However, there were no group differences

13

269   found in the metaphysis. Data suggest deformities are worse near the articulating surface, likely

270   due to the greater amount of mechanical loading. Following analyses of the humerus, this study

271   investigated the effects of BPBI on the scapula. Of the three zones, zone 3 had the least robust

272   metrics. Zone 3 resides closest to the articulating surface, also suggesting greater deformities near

273   the articulating surface. When compared to the humerus, the scapula had greater disparities,

274   especially in the trabecular architecture. The large amount of alterations in scapular microstructure

275   suggest the humerus is not affected the most post-injury.

276   Although the humerus was less affected than the scapula, some microstructure metrics of

277   the epiphysis did seem to correlate or trend towards a correlation with the scapular zone 3

278   microstructure metrics. The metrics most correlated were the scapular zone 3 tissue mineral

279   density with epiphyseal trabecular bone architecture metrics and bone mass metrics and the

280   epiphyseal degree of anisotropy with zone 3 trabecular bone architecture metrics and bone mass

281   metrics. This suggests that when the trabecular bone in the humeral epiphysis becomes less robust,

282   the tissue mineral density in the scapular neck is also altered. It also suggests that when the

283   trabecular bone in the scapular neck becomes less robust, the degree of anisotropy in the humeral

284   epiphysis increases, meaning the trabecular bone orientation is more anisotropic. However, the

285   trabecular metrics as a whole are not changing similarly between the two regions. Therefore, the

286   mechanical loading may be affecting one bone more than the other and not to a similar degree.

287   Based on previous studies of human trabecular bone, even modest decreases in bone tissue

288   mineralization, such as the ~4% drop in TMD in the scapular zone 2, can lead to much greater

289   reductions in the tissue modulus and strength (Carter 1977),[23] which will weaken bone's overall

290   resistance to loading. Diminished physical properties of trabeculae (e.g., BV/TV, Tb.N, Tb.Th, or

291   Tb.Sp) can also increase fracture risk, as has been shown in other clinical cases like osteoporosis[24]

292   (Parfitt *et al.*, 1983)[38] and osteopenia (Stein *et al*., 2014).[25] Reduced Tb.N is a significant

293   predictor of vertebral fracture in middle-aged men diagnosed with osteopenia (Legrand *et al*.,

294   2000).[26][40] Although it has not been studied, our findings suggest that the alterations in trabecular

295   architecture following BPBI may decrease load-bearing capacity in the affected limb and increase

296   the risk of bone fracture in the humerus and scapula due to mechanical loading exceeding the

297   altered load-bearing threshold level.

298   We acknowledge that limitations exist within our study design. First, rats are weight

299   bearing quadrupeds throughout their lifetime, while human infants outgrow crawling. The different

300   relative time-periods of walking on forelimbs and hindlimbs between rats and humans may induce

301   differing mechanical loading. However, neither rats nor humans use their affected arm following

302   injury, and the murine model has been proven to produce consequences similar to humans in terms

303   of severity (Li 2010).[27]

304   In addition, this study was not powered to detect the small differences measured in

305   trabecular TMD and Tb.Th, but a post-hoc power analysis revealed that the measure differences

306   would require a sample size of 16 per group for TMD and 14 per group for Tb.Th to reach statistical

307   significance ($p < 0.05$). While micro-CT analyses reveal trabecular bone changes following

308   neurectomy, the mechanisms underlying these changes are not well understood. Histological

309   assessments of bone remodeling may provide additional insight into the underlying mechanisms

310   driving the trabecular bone changes with peripheral nerve injury.

311   Finally, nerve injury is complex. Whether nerve injury directly influences skeletal

312   development remains an open question, one that is also confounded by cellular crosstalk between

313   muscle and bone cells (Hamrick, McNeil, & Patterson, 2010).[28] A recent study reported that

314   location of nerve injury with respect to the dorsal root ganglion can have different effects on

315   muscle spindle preservation and longitudinal muscle growth (Nikolaou *et al.*, 2015),[18] which

316   motivates the need to examine these effects in more detail. Moreover, almost nothing is known

317   about the timing of nerve injury during postnatal development on the serial progression of muscle

318   and bone deficits following injury, which may provide essential information that could lead to

319   improved therapies in human patients.

320   Our study reveals significantly altered trabecular bone properties in regions of the shoulder

321   underlying the glenohumeral joint surfaces, particularly in the scapula. While fracture more

322   commonly occurs in the clavicle as opposed to the glenohumeral bones (Ogden, 2000),[29]

323   following BPBI, our study suggests that altered trabecular bone mineralization and microstructure

324   in the glenohumeral bones may compromise bone strength during the critical period of postnatal

325   skeletal development. Longitudinal studies are necessary to assess whether increased risk of

326   fracture is an overlooked, unmet clinical need. Shoulder joint health in BPBI patients may benefit

327   from the development of better post-injury care plans that target the maintenance of underlying

328   trabecular bone. Our study is the first to characterize trabecular microstructure in the humeral

329   metaphyseal and the glenoid fossa region of the scapula, giving insight into the underlying

330   microstructure of the glenohumeral as a whole post-injury.

331

References

1. Natural_history_of_obstetric_b.pdf.

2. Al-Qattan MM. Classification of Secondary Shoulder Deformities in Obstetric Brachial Plexus Palsy. J. Hand Surg. 2003 Oct;28(5):483–6.

3. Nikolaou S, Peterson E, Kim A, Wylie C, Cornwall R. Impaired Growth of Denervated Muscle Contributes to Contracture Formation Following Neonatal Brachial Plexus Injury: J. Bone Jt. Surg. 2011 Mar;93(5):461–70.

4. Crouch DL, Plate JF, Li Z, Saul KR. Computational Sensitivity Analysis to Identify Muscles That Can Mechanically Contribute to Shoulder Deformity Following Brachial Plexus Birth Palsy. J. Hand Surg. 2014 Feb;39(2):303–11.

5. Crouch DL, Hutchinson ID, Plate JF, Antoniono J, Gong H, Cao G, Li Z, Saul KR. Biomechanical Basis of Shoulder Osseous Deformity and Contracture in a Rat Model of Brachial Plexus Birth Palsy: J. Bone Jt. Surg. 2015 Aug;97(15):1264–71.

6. Cheng W, Cornwall R, Crouch DL, Li Z, Saul KR. Contributions of Muscle Imbalance and Impaired Growth to Postural and Osseous Shoulder Deformity Following Brachial Plexus Birth Palsy: A Computational Simulation Analysis. J. Hand Surg. 2015 Jun;40(6):1170–6.

7. Vico L, Collet P, Guignandon A, Lafage-Proust M-H, Thomas T, Rehailia M, Alexandre C. Effects of long-term microgravity exposure on cancellous and cortical weight-bearing bones of cosmonauts. The Lancet. 2000 May;355(9215):1607–11.

8. Kazakia GJ, Tjong W, Nirody JA, Burghardt AJ, Carballido-Gamio J, Patsch JM, Link T, Feeley BT, Benjamin Ma C. The influence of disuse on bone microstructure and mechanics assessed by HR-pQCT. Bone. 2014 Jun;63:132–40.

354   9.   Eser P, Schiessl H, Willnecker J. Bone loss and steady state after spinal cord injury: A

355   cross-sectional study using pQCT. :3.

356   10. Kim HM, Galatz LM, Patel N, Das R, Thomopoulos S. Recovery Potential After Postnatal

357   Shoulder Paralysis: An Animal Model of Neonatal Brachial Plexus Palsy. J. Bone Jt. Surg.-

358   Am. Vol. 2009 Apr;91(4):879–91.

359   11. Kim HM, Galatz LM, Das R, Patel N, Thomopoulos S. Musculoskeletal deformities

360   secondary to neurotomy of the superior trunk of the brachial plexus in neonatal mice. J.

361   Orthop. Res. 2010 Mar 11;28(10):1391–8.

362   12. Potter R, Havlioglu N, Thomopoulos S. The developing shoulder has a limited capacity to

363   recover after a short duration of neonatal paralysis. J. Biomech. 2014 Jul;47(10):2314–20.

364   13. [Frost 1994] wolf's law.pdf.

365   14. Turner CH. Three rules for bone adaptation to mechanical stimuli. Bone. 1998

366   Nov;23(5):399–407.

367   15. Reading BD, Laor T, Salisbury SR, Lippert WC, Cornwall R. Quantification of Humeral

368   Head Deformity Following Neonatal Brachial Plexus Palsy: J. Bone Jt. Surg.-Am. Vol.

369   2012 Sep;94(18):e136-1–8.

370   16. Waters PM, Smith GR, Jaramillo D. Glenohumeral Deformity Secondary to Brachial

371   Plexus Birth Palsy: J. Bone Jt. Surg. 1998 May;80(5):668–77.

372   17. Li Z, Ma J, Apel P, Carlson CS, Smith TL, Koman LA. Brachial Plexus Birth Palsy–

373   Associated Shoulder Deformity: A Rat Model Study. J. Hand Surg. 2008 Mar;33(3):308–

374   12.

375 18. Nikolaou S, Hu L, Cornwall R. Afferent Innervation, Muscle Spindles, and Contractures

376   Following Neonatal Brachial Plexus Injury in a Mouse Model. J. Hand Surg. 2015

377   Oct;40(10):2007–16.

378 19. Crouch DL, Hutchinson ID, Plate JF, Antoniono J, Gong H, Cao G, Li Z, Saul KR.

379   Biomechanical Basis of Shoulder Osseous Deformity and Contracture in a Rat Model of

380   Brachial Plexus Birth Palsy: J. Bone Jt. Surg.-Am. Vol. 2015 Aug;97(15):1264–71.

381 20. Kothary S, Rosenberg ZS, Poncinelli LL, Kwong S. Skeletal development of the glenoid

382   and glenoid–coracoid interface in the pediatric population: MRI features. Skeletal Radiol.

383   2014 Sep;43(9):1281–8.

384 21. Hildebrand T, Rüegsegger P. Quantification of Bone Microarchitecture with the Structure

385   Model Index. Comput. Methods Biomech. Biomed. Engin. 1997 Jan;1(1):15–23.

386 22. Bouxsein ML, Boyd SK, Christiansen BA, Guldberg RE, Jepsen KJ, Müller R. Guidelines

387   for assessment of bone microstructure in rodents using micro-computed tomography. J.

388   Bone Miner. Res. 2010 Jun 7;25(7):1468–86.

389 23. The compressive behavior of bone as a two-phase porous structure.pdf.

390 24. Parfitt AM, Mathews CH, Villanueva AR, Kleerekoper M, Frame B, Rao DS. Relationships

391   between surface, volume, and thickness of iliac trabecular bone in aging and in

392   osteoporosis. Implications for the microanatomic and cellular mechanisms of bone loss. J.

393   Clin. Invest. 1983 Oct;72(4):1396–409.

394 25. Stein EM, Kepley A, Walker M, Nickolas TL, Nishiyama K, Zhou B, Liu XS, McMahon

395   DJ, Zhang C, Boutroy S, Cosman F, Nieves J, Guo XE, Shane E. Skeletal Structure in

396   Postmenopausal Women With Osteopenia and Fractures Is Characterized by Abnormal

397   Trabecular Plates and Cortical Thinning: SKELETAL STRUCTURE IN OSTEOPENIC

398   POSTMENOPAUSAL WOMEN. J. Bone Miner. Res. 2014 May;29(5):1101–9.

399 26. Legrand E, Chappard D, Pascaretti C, Duquenne M, Krebs S, Rohmer V, Basle M-F,

400   Audran M. Trabecular bone microarchitecture, bone mineral density, and vertebral fractures

401   in male osteoporosis. J. Bone Miner. Res. 2000;15(1):13–19.

402 27. Li Z, Barnwell J, Tan J, Koman LA, Smith BP. Microcomputed Tomography

403   Characterization of Shoulder Osseous Deformity After Brachial Plexus Birth Palsy: A Rat

404   Model Study: J. Bone Jt. Surg.-Am. Vol. 2010 Nov;92(15):2583–8.

405 28. Hamrick MW, McNeil PL, Patterson SL. Role of muscle-derived growth factors in bone

406   formation. 2013;12.

407 29. John A. Ogden. Skeletal injury in the child. 3rd ed. New York: Springer-Verlag New York;

408   2000.

409

410 **Figures**

411
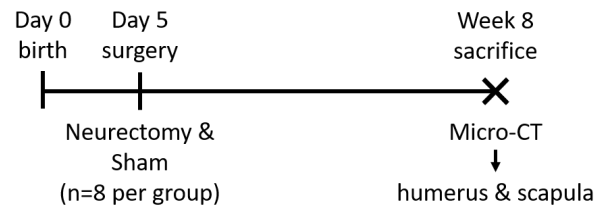
413 **Figure 1.** Overview of study timeline. Interventions were performed at the same timepoint.

414 Analyses will be performed following sacrifice at week 8.

21

415
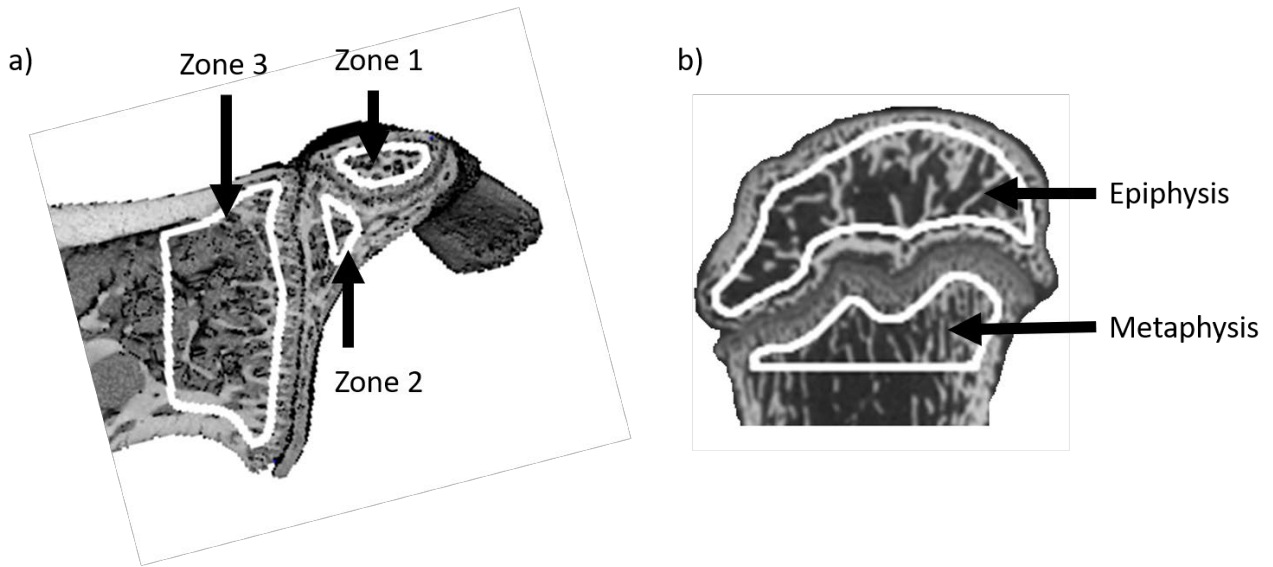
Figure 2. Trabecular bone volumes of interest (outlined in white) in the a) scapula and b)

humerus, selected within different ossification centers, or zones.
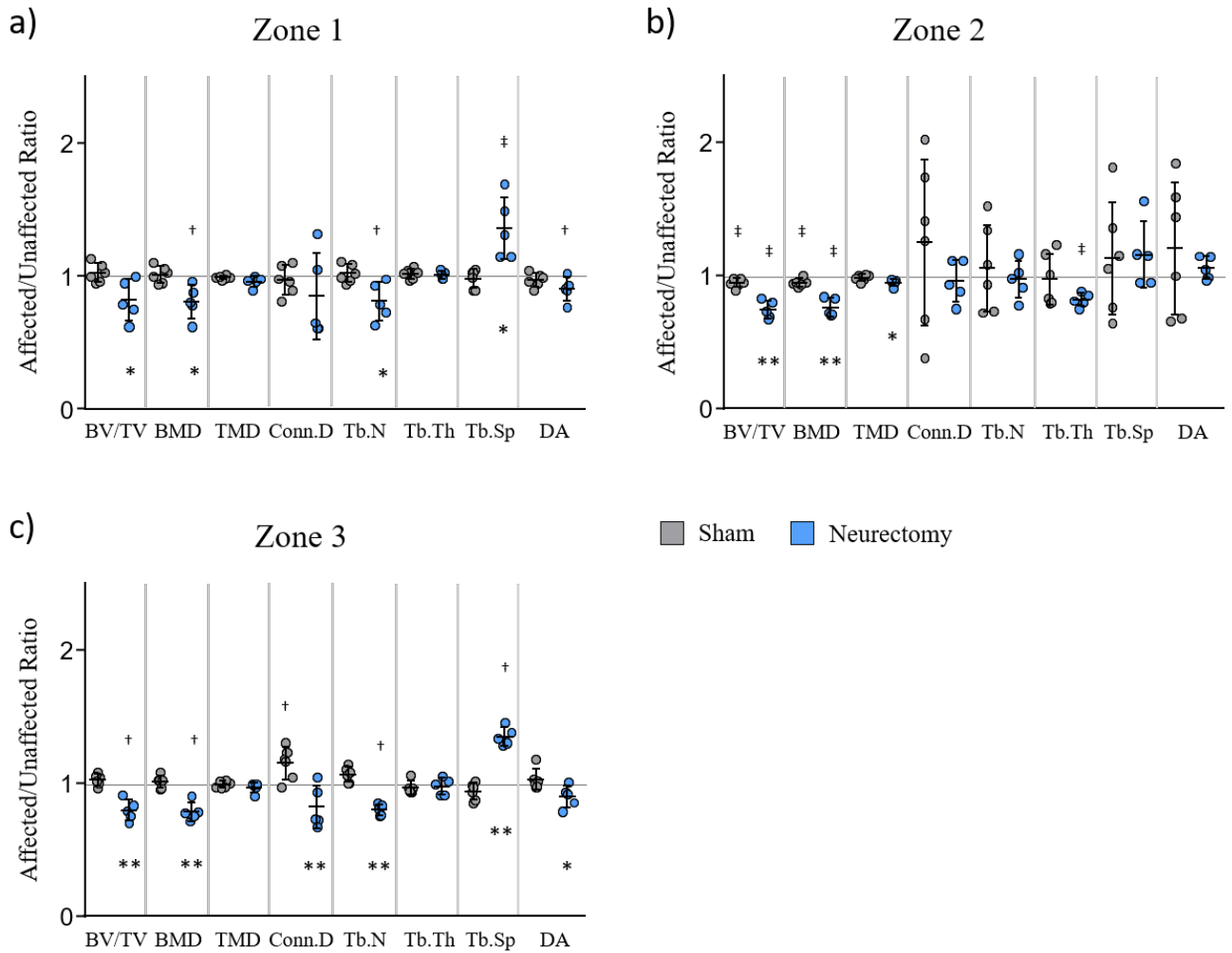
Figure 3. Trabecular bone metrics in the scapula. All three zones exhibited differences in trabecular microstructure in the neurectomy group with zone 3 portraying the most differences. a) Zone 1 shows decreased BV/TV, BMD, and Tb.N, and increased Tb.Sp. b) Zone 2 shows decreased BV/TV, BMD, and TMD. c) Zone 3 shows decreased BV/TV, BMD, Conn.D, Tb.N, and DA, and increased Tb.Sp. $^\dagger p < 0.05$, $^\ddagger p < 0.01$ affected vs. unaffected limb, $*p < 0.05$, $**p < 0.01$ neurectomy vs. sham.

23
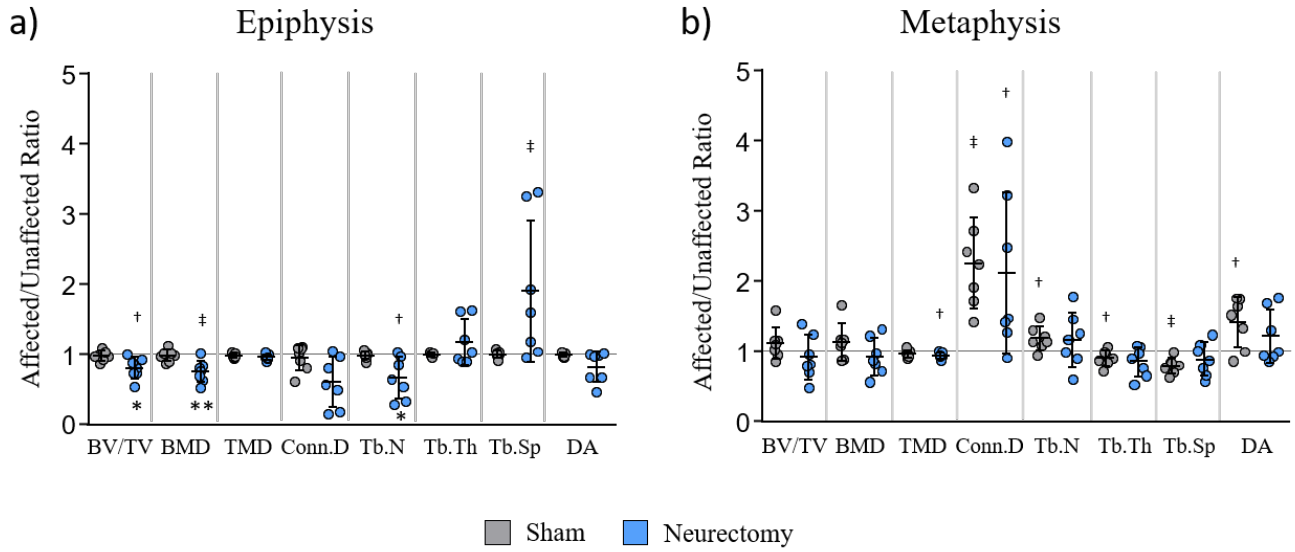
Figure 4. Trabecular bone metrics in the humerus. a) The epiphysis showed decreased BMD, Conn.D, and Tb.N in the neurectomy group. b) The metaphysis showed no significant differences between groups. $^{\dagger}p < 0.05$, $^{\ddagger}p < 0.01$ affected vs. unaffected limb, $*p < 0.05$, $**p < 0.01$ neurectomy vs. sham.

430 **Tables**

431

432 **Table 1.** Trabecular bone metrics in the scapula volumes of interest (VOI), expressed as percent

433 difference between the affected and the unaffected side. $^{\#}p < 0.1$, $^{*}p < 0.05$, $^{**}p < 0.01$ for affected

434 vs. unaffected.

Surgery	VOI	Affected Side vs. Unaffected Side (%)							
		BV/TV	BMD	TMD	Conn.D	Tb.N	Tb.Th	Tb.Sp	DA
Sham	Zone 1	3.9	2.6	-1.2	-3.1	3.5	2.9	-3.4	-4.3
	Zone 2	-5.4**	-5.2**	-2.1	22.4	7.8	-3.7	12.4	30.6
	Zone 3	1.9	0.6	-1.6	11.5*	4.8$^{\#}$	-2.8	-5.0$^{\#}$	3.6
Neurectomy	Zone 1	-17.8$^{\#}$	-19.4*	-3.9	-15.2	-18.8*	0.9	44.0**	-9.7*
	Zone 2	-25.6**	-23.9**	-5.3$^{\#}$	-4.3	-3.0	-18.3**	15.6	5.6
	Zone 3	-20.5*	-21.8*	-3.5	-18.2$^{\#}$	-20.1*	-2.6	34.8*	-10.2

435

436 **Table 2.** Trabecular bone metrics in the humerus volumes of interest (VOI), expressed as percent

437 difference between the affected and the unaffected side. $^{\#}p < 0.1$, $*p < 0.05$, $**p < 0.01$ for affected

438 vs. unaffected.

Surgery	VOI	Affected Side vs Unaffected Side (%)							
		BV/TV	BMD	TMD	Conn.D	Tb.N	Tb.Th	Tb.Sp	DA
Sham	Epiphysis	0.5	1.2	-0.9	0.5	0.2	0.1	-0.9	0.4
	Metaphysis	14.9	18.5	-2.5	139.2**	16.3*	-6.2#	-18.3**	44.9*
Neurectomy	Epiphysis	-19.1*	-24.3**	-3.6#	-39.2	-33.4#	17.6	90.1**	-17.2
	Metaphysis	-8.1	-6.8	-5.7*	112.0*	16.9	-14.0	-10.9	21.8

439

440 **Table 3.** Pearson's correlation coefficients (r) and associated p-values for correlations of trabecular

441 density and microstructure of the epiphysis and scapular zone 3 in the neurectomy groups. $p < 0.05$

442 in bold.

			Zone3							
			BV/TV	BMD	TMD	ConnD	Tb.N	Tb.Th	Tb.Sp	DA
Epiphysis	BV/TV	r	-0.049	0.148	0.837	0.005	-0.270	-0.275	0.349	-0.506
		p	0.938	0.812	0.077	0.994	0.660	0.655	0.565	0.385
	BMD	r	-0.079	0.115	0.816	0.059	-0.280	-0.384	0.380	-0.554
		p	0.900	0.854	0.092	0.925	0.646	0.523	0.528	0.333
	TMD	r	-0.055	0.082	0.721	0.250	0.043	-0.618	0.081	-0.493
		p	0.930	0.895	0.169	0.685	0.946	0.266	0.897	0.399
	ConnD	r	0.097	0.285	**0.913**	0.170	-0.090	-0.309	0.185	-0.395
		p	0.877	0.642	**0.030**	0.785	0.888	0.613	0.766	0.512
	Tb.N	r	0.247	0.428	**0.946**	0.311	0.005	-0.280	0.105	-0.266
		p	0.688	0.472	**0.015**	0.610	0.994	0.648	0.867	0.665
	Tb.Th	r	0.070	0.248	0.696	-0.130	-0.360	0.135	0.377	-0.263
		p	0.912	0.688	0.192	0.839	0.553	0.828	0.532	0.669
	Tb.Sp	r	-0.356	-0.525	**-0.978**	-0.400	-0.140	0.251	0.035	0.157
		p	0.557	0.363	**0.004**	0.509	0.817	0.684	0.956	0.801
	DA	r	0.873	0.840	0.462	0.648	**0.973**	0.250	**-0.960**	0.766
		p	0.054	0.075	0.433	0.237	**0.005**	0.685	**0.010**	0.131

443

444 **Table 4.** Pearson's correlation coefficients (r) and associated p-values for correlations of trabecular density and microstructure with

445 macrostructure metrics in BPBI rat shoulders. p<0.05 in bold.

			Bone Density and Microstructure							
			Scapula						Humerus	
			Zone 1	Zone 2	Zone 3			Epiphysis		Metaphysis
	Morphology[a]		Tb.Sp	BV/TV	BV/TV	Tb.N	Tb.Sp	Tb.Th	TMD	Tb.Th
Glenoid Fossa	Version	r	-0.47	**0.17**	0.41	0.44	-0.39	0.42	0.51	0.45
		p	0.12	**0.030**	0.17	0.16	0.21	0.18	0.094	0.14
	Inclination	r	**-0.78**	**0.79**	**0.79**	**0.84**	**-0.87**	**0.86**	**0.59**	**0.82**
		p	**0.0026**	**0.0024**	**0.0023**	**0.0006**	**0.0003**	**0.0004**	**0.045**	**0.0011**
Humeral Head	Anteroposterior Subluxation	r	0.55	**-0.62**	**-0.59**	-0.41	0.39	-0.55	-0.27	**-0.59**
		p	0.064	**0.031**	**0.042**	0.19	0.22	0.063	0.40	**0.043**
	Superoinferior Translation	r	**-0.71**	**0.77**	**0.89**	**0.79**	**-0.80**	**0.91**	**0.60**	**0.89**
		p	**0.0093**	**0.0031**	**0.0001**	**0.0021**	**0.0019**	**<0.0001**	**0.0384**	**<0.0001**

[a] For gross morphological measurements of the scapula and humerus, see Crouch *et al.*, 2015.

446